Design, Sensing, and Planning: Fundamentally Coupled Problems for Continuum Robots

Arthur W. Mahoney, Trevor L. Bruns, Ron Alterovitz and Robert J. Webster III

1 Introduction

Continuum robot systems have been created for use in a large variety of practical applications, including underwater manipulation, nuclear reactor repair, sanding, spray painting, and medical applications [9, 47]. A variety of continuum-robot devices exist, include multi-backbone devices [48], tendons routed around a backbone [30], concentrically-nested elastic tubes [12, 31], pneumatic actuators [18], shape-memory-based designs [1, 33], and combinations thereof. Some of these are illustrated in Fig. 1a–d. Each type of continuum robot presents a variety of physical design parameters, including diameter, segment number and length, material properties, and actuation systems, among others [47].

The typical process for designing and using a continuum robot in a new application typically involves three discrete steps that are addressed serially. First, one designs the physical robot to be suitable for the task, i.e. able to reach the desired workspace, carry the desired payload, etc. Attention is then turned toward sensing. Sensors are

This material is based upon work supported by the National Institutes of Health under awards R21 EB017952 and R01 EB017467, and the National Science Foundation under award IIS-1054331.

A.W. Mahoney (✉) · T.L. Bruns · R.J. Webster III
Department of Mechanical Engineering, Nashville, TN 37235, USA
e-mail: art.mahoney@vanderbilt.edu

T.L. Bruns
e-mail: trevor.l.bruns@vanderbilt.edu

R.J. Webster III
e-mail: robert.webster@vanderbilt.edu

R. Alterovitz
Department of Computer Science, University of North Carolina,
Chapel Hill, NC 27599, USA
e-mail: ron@cs.unc.edu

A. Bicchi and W. Burgard (eds.), *Robotics Research*, Springer Proceedings in Advanced Robotics 2, DOI 10.1007/978-3-319-51532-8_17

selected, which may be integrated into the robot, or located off-board. Lastly, given the physical robot, the motion of the robot is planned to accomplish the desired task. In what follows, we briefly discuss the state-of-the-art in these areas and describe the coupling between design, sensing, and planning.

Research on physical robot design has focused largely on developing general purpose manipulators of various types [16, 47]. Intense design effort has been focused on a wide variety of medical applications, which has resulted in many new physical continuum robot structures [9], including concentric precurved tubes [13], which will be used as an example later in this paper. Computational design algorithms are also increasingly being used in the design of concentric-tube robots [4, 8, 40], and similar techniques could be applicable to task-specific design of other types of continuum robot.

Selecting and integrating sensors in continuum robots can be challenging. Often, most of the continuum robot's volume is reserved for actuation, and little room is left for sensing – particularly in the small diameter designs used in medical applications. Many sensing methods have been developed that measure the pose at a discrete points on the continuum robot's backbone such as electromagnetic trackers [17], mechanical strain of the backbone such as the fiber Bragg gratings [29, 32], and the internal moments of a continuum robot's backbone [49]. To keep the continuum-robot diameter small, these sensors are integrated into the robot's mechanical structure when possible. Vision-based methods are also possible and X-ray/CT-imaging [21], ultrasound approaches [19, 23], and optical cameras [5, 15] have been applied. Some of the above sensing systems, which can be used to detect the shape/states of a continuum robot, are illustrated in Fig. 1f–i.

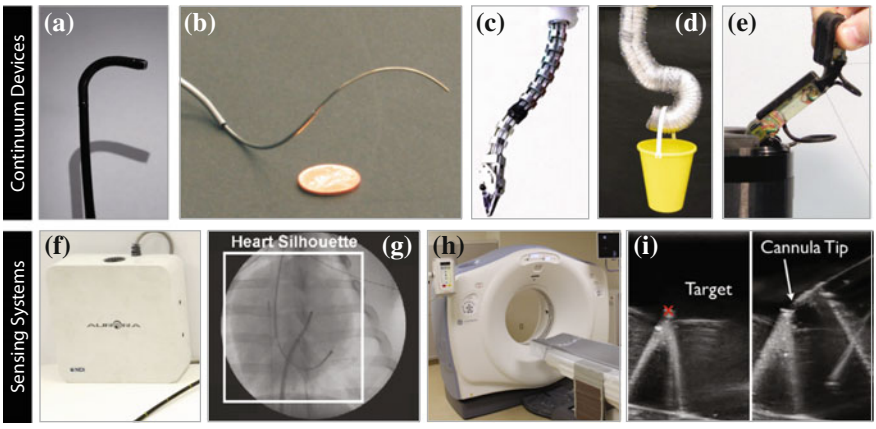

Fig. 1 Continuum robots include devices such as **a** tendon-actuated endoscopes, **b** concentric-tube robots, **c** pushrod-actuated devices, e.g., [48], **d** pneumatic robots, e.g., [18], **e** and some compliant graspers may also fall under this classification, such as that of [24]. Some approaches to sensing the state of continuum robots include **a** magnetic tracking such as the NDI Aurora system, **g–h** X-ray or CT imaging such as [19], and **i** three-dimensional (3D) ultrasound, e.g., [37]

Planning the motion of a continuum robot can enable the robot to automatically reach a specified target while avoiding obstacles in the environment. Motion planning for continuum robots such as concentric-tube robots is challenging because, compared to traditional multi-link manipulators, their kinematics are typically more expensive to evaluate and their motion is subject to substantial uncertainty. Motion planning algorithms for concentric-tube robots include fast motion planning by assuming simplified kinematics [22, 43], noninteractive motion planning using accurate kinematic models [39], interactive-rate motion planning using accurate kinematic modeling via precomputation [41], and motion planners that explicitly consider uncertainty in motion and sensing [36]. Motion planners can also assist in the context of teleoperation, where a fast, real-time motion planner can automatically move the robot's end-effector in response to user commands in a manner that ensures the entire curvilinear shaft avoids obstacles [42].

Recent research in continuum robotics is showing that there are advantages to solving sensing-and-planning problems and design-and-sensing problems simultaneously. In the case of motion planning for continuum robots, for example, effective obstacle avoidance requires accurate estimation of the shape of the robot, and simultaneously planning the motion of the robot and the placement of moveable sensors has the potential to improve task success rates [44]. Motion planning can also help inform the design of concentric-tube robots, e.g., by identifying stable configurations [3] and in optimizing the design of concentric tubes [2, 40].

In this paper argue that design, sensing, and planning are fundamentally coupled problems for continuum robots, and that the interaction between these three problems can be understood through the application of statistical state estimation.

2 Kinematics of a Continuum Robot

We use a notation where scalars are denoted by lower-case standard font (e.g., s), vectors are denoted by bold, lower-case fonts (e.g., $\boldsymbol{x}$), matrices are upper-case standard-font (e.g., M). For compactness, we use subscript notation to denote function arguments. For example, if a vector is a function of s, then it is written as $\boldsymbol{x}_s$.

The kinematics of a continuum robot describe both the continuous spatial transition of the states of the robot's backbone, parameterized by the distance s along the robot's backbone, as well as the continuous temporal transition of the states as an input varies in time. For this present work, we only consider the spatial kinematics that govern how the states $\boldsymbol{x}_s$, parameterized by arc-length distance s, vary along the robot's backbone. We assume that the arc-length distance s falls in the range $[0, \ell]$, where $s = 0$ denotes the proximal end of the continuum robot (i.e., the base) and $s = \ell$ denotes the distal end (i.e., the tip). The state of a continuum robot can include, for example, internal torsional moments and pose of the backbone in $SE(3)$, all of which vary continuously along the length of the backbone with the parameter s. The backbone may be a physical structure as is the case for concentric-tube robots, and

some tendon actuated continuum robots, or the backbone could be a theoretical curve used as a reference location with respect to the robot's body.

If the continuum robot is in equilibrium (i.e., quasi static), then the spatial kinematics of a continuum robot can be described by the two-point boundary-value differential equation in arc-length s along the the robot's body:

$$\boldsymbol{x}_s' = \boldsymbol{f}\left(\boldsymbol{x}_s, s\right), \tag{1}$$

where $'$ is an arc-length differentive, and with constraints and inputs of the form

$$\boldsymbol{b}_0(\boldsymbol{x}_0) = \boldsymbol{0} \qquad \boldsymbol{b}_\ell(\boldsymbol{x}_\ell) = \boldsymbol{0} \qquad \boldsymbol{u}(\boldsymbol{x}_0) = \boldsymbol{0} \tag{2}$$

where $\boldsymbol{b}_0$ and $\boldsymbol{b}_\ell$ define the stationary proximal and distal boundary conditions, respectively, and $\boldsymbol{u}$ defines the system input. The proximal boundary condition can constrain properties such as the proximal pose in $SE(3)$ of a continuum robot's body. The distal boundary conditions can constrain properties such as the torsional moment of a concentric-tube robot's tubes, and the net force and moment applied to the end-effector platform of a parallel continuum manipulator by its rod-actuators [7]. The input function $\boldsymbol{u}(\boldsymbol{x}_0)$ operates on the proximal state and can define the proximal tendon displacement of a tendon-actuated device or the proximal twist angles of the tubes comprising a concentric-tube robot.

In this paper, we use concentric-tube robots as examples. Concentric-tube robots, shown in Fig. 1b, consist of precurved, elastic tubes that move in a tentacle-like fashion when the tubes are rotated and translated relative to each other. The states of an unloaded concentric-tube robot are the tubes' twist angles $\boldsymbol{\psi}_s$, their arc-length rates-of-change $\boldsymbol{\psi}_s'$, the arc-length position of each tube $\boldsymbol{\sigma}_s$ relative to the tubes' proximal ends, and backbone position $\boldsymbol{p}_s$ and orientation R_s.

The kinematics of an n-tube concentric-tube robot is governed by

$$^i\psi_s'' = -\boldsymbol{u}_s^{\mathsf{T}\,i}K_s\left(\partial R(^i\psi_s)\right)^i\boldsymbol{u}_s^* \tag{3a}$$

$$^i\sigma_s' = 1 \tag{3b}$$

$$\boldsymbol{p}_s' = R_s\boldsymbol{z} \tag{3c}$$

$$R_s' = R_s S(\boldsymbol{u}_s) \tag{3d}$$

where $\boldsymbol{u}_s$ is the frame curvature, the bending and torsional stiffnesses of tube i are packed in the diagonal matrix ^iK_s, the matrix $\partial R(^i\psi_s) = \partial R(^i\psi_s)/\partial {}^i\psi_s$ where $R(^i\psi_s)$ is the standard z-axis rotation matrix by the angle $^i\psi_s$, $^i\boldsymbol{u}_s^*$ is the tube precurvature, and $S(\boldsymbol{u}_s)$ is the skew-symmetric matrix representing the cross-product operation. Further details can be found in [12, 31].

The proximal boundary conditions are

$$\boldsymbol{p}_0 = \boldsymbol{0}, \quad R_0 - I = 0, \tag{4}$$

and the distal boundary condition is

$$\boldsymbol{\psi}'_{\ell} = \mathbf{0}, \tag{5}$$

assuming that when a tube is not physically present at an arc-length, it has infinite torsional stiffness and zero bending stiffness. The inputs are

$$\boldsymbol{\psi}_0 - \boldsymbol{\alpha} = \mathbf{0}, \quad \boldsymbol{\sigma}_0 - \boldsymbol{\gamma} = \mathbf{0}, \tag{6}$$

where $\boldsymbol{\alpha}$ and $\boldsymbol{\gamma}$ are the tubes' *actuator* rotation angles and translations, respectively.

3 State Estimation for Continuum Robots

In this paper, we argue that design, sensing, and planning are fundamentally coupled problems for continuum robots, and that statistical state estimation can be used to understand the interaction between these three problems. The goal of statistical state estimation is to infer a continuum robot's state that is most likely given the prior model (1)–(2) and sensor observations, in the presence of uncertainty in the process, observations, and boundary constraints. We assume that beliefs can be modeled with Gaussian distributions, denoted with $\mathcal{N}(\boldsymbol{x}, \Sigma)$, having mean $\boldsymbol{x}$ and covariance Σ.

Uncertainty in the spatial kinematics of a continuum robot is modeled using a spatial stochastic process given by

$$\boldsymbol{x}'_s = \boldsymbol{f}(\boldsymbol{x}_s, s) + \boldsymbol{q}_s \tag{7}$$

with uncertain constraints and inputs of the form

$$\boldsymbol{b}_0(\boldsymbol{x}_0) = \boldsymbol{w}_0 \qquad \boldsymbol{b}_\ell(\boldsymbol{x}_\ell) = \boldsymbol{w}_\ell \qquad \boldsymbol{u}(\boldsymbol{x}_0) = \boldsymbol{v} \tag{8}$$

where $\boldsymbol{q}_s \sim \mathcal{N}(\mathbf{0}, Q_s)$ represents uncertainty in the process and is independent in arc-length. Uncertainty in the boundary conditions is accounted for by $\boldsymbol{w}_0 \sim \mathcal{N}(\mathbf{0}, W_0)$ and $\boldsymbol{w}_\ell \sim \mathcal{N}(\mathbf{0}, W_\ell)$, which are independent. Uncertainty in the input is represented by $v \sim \mathcal{N}(\mathbf{0}, V)$. Uncertainty in the proximal boundary condition could model uncertainty in the proximal pose of a continuum robot. Uncertainty in the distal boundary condition could model uncertainty in the distal torsional moment for a concentric-tube robot, which is ideally moment-free without applied loading.

We denote a set of time-invariant observation functions $\boldsymbol{h}_{s_1}, \ldots, \boldsymbol{h}_{s_m}$ to be defined at discrete arc-lengths $s_1, \ldots, s_m$ as

$$\boldsymbol{y}_{s_i} = \boldsymbol{h}_{s_i}(\boldsymbol{x}_{s_i}) + \boldsymbol{z}_{s_i}, \tag{9}$$

where i indicates the i^{th} observation and $i = 1, \ldots, m$. Note that we do not assume the measurements are evenly spaced or that the dimension of each measurement is the same (i.e., the measurements can be gathered by a heterogeneous collection of

sensors placed arbitrarily along the length of the continuum robot). The observations are subject to additive noise $z_{s_i} \sim N(\mathbf{0}, Z_{s_i})$, and are mutually uncorrelated.

3.1 Spatial Statistical Estimation

Statistical estimation infers the continuum robot's state-curve given the model (7), uncertain inputs and constraints (8), and all noisy sensor observations on the robot's body. Estimation requires that the states be observable from sensor measurements [34]. The best estimate is the smoothed estimate, denoted by $\mathcal{N}(\bar{\boldsymbol{x}}_s, \bar{P}_s)$ with expected value $\bar{\boldsymbol{x}}_s$ and covariance $\bar{P}_s$, and can be approximated in a two-step procedure:

(1) The first step recursively computes the *posterior* estimate at any arc-length s, denoted by $\mathcal{N}(\tilde{\boldsymbol{x}}_s, \tilde{P}_s)$, which incorporates the sensor observations in the arc-length interval $[0, s]$, the proximal boundary constraints $\boldsymbol{b}_0$, and the inputs $\boldsymbol{u}$. The *posterior* estimate is found using an extended Kalman filter that has become ubiquitous throughout robotics [38], and is obtained by continuously propagating a *prior* state estimate, denoted by $\mathcal{N}(\hat{\boldsymbol{x}}_s, \hat{P}_s)$, down the length of the robot's backbone using the extended Kalman-Bucy equations, and updating it at measurement locations s_i to form the *posterior* estimate. The *prior* state estimate is the belief given all sensor measurements obtained in the arc-length interval $[0, s)$. If no sensor measurement is present at s, then the *prior* and *posterior* estimates are the same.

The *prior* estimate is propagated by piecewise-integrating the equations

$$\hat{\boldsymbol{x}}_s' = \boldsymbol{f}(\hat{\boldsymbol{x}}_s, s) \tag{10}$$

$$\hat{P}_s' = F_s \hat{P}_s + \hat{P}_s F_s^{\mathsf{T}} + Q_s \tag{11}$$

from $s = 0$ to ℓ in the intervals $[0, s_1], [s_{i-1}, s_i], \ldots, [s_m, \ell]$. The initial conditions, $\hat{\boldsymbol{x}}_0$ and $\hat{P}_0$, represent prior information that could be found by solving (1)–(2).

The *prior* estimate is updated to form the *posterior* estimate with a Kalman update at every sensor observation at arc-lengths $s_1 \cdots s_m$, of the form

$$\hat{S}_{s_i} = \hat{H}_{s_i} \hat{P}_{s_i} \hat{H}_{s_i}^{\mathsf{T}} + Z_{s_i} \tag{12}$$

$$\hat{K}_{s_i} = \hat{P}_{s_i} \hat{H}_{s_i}^{\mathsf{T}} \hat{S}_{s_i}^{-1} \tag{13}$$

$$\tilde{\boldsymbol{x}}_{s_i} = \hat{\boldsymbol{x}}_{s_i} + \hat{K}_{s_i} \left(\boldsymbol{y}_{s_i} - \boldsymbol{h}_{s_i}(\hat{\boldsymbol{x}}_{s_i}) \right) \tag{14}$$

$$\tilde{P}_{s_i} = (I - \hat{K}_{s_i} \hat{H}_{s_i}) \hat{P}_{s_i}. \tag{15}$$

The inputs and boundary conditions (8) can be incorporated using the Kalman update Eqs. (12)–(15). For example, the distal boundary condition can be incorporated as a Kalman update with $\hat{H}_{s_i}$, Z_{s_i}, and $\boldsymbol{y}_{s_i}$ replaced with the matrix $\partial \boldsymbol{b}_\ell / \partial \boldsymbol{x}_\ell$, W_ℓ and $\mathbf{0}$, respectively. In theory, the incorporation of constraints in this way also works if there is no uncertainty in the constraints (i.e., the constraint covariances,

W_0 or W_ℓ, are not invertible). Care must be taken in this case since numerical issues while integrating (11) may result in eigenvalues of the estimate covariance becoming negative, making the covariance no longer positive-definite. In this case, square-root formulations of the filtering equations can be used to increase precision and ensure that the positive semidefinite-ness is preserved [10].

(2) The *posterior* estimate is then used by the second step, which computes the state estimate at arc-length s that incorporates all sensor observations everywhere on the robot, the proximal and distal boundary constraints, and the inputs using an extended form of a Kalman smoother. Smoothing is frequently used as a method for batch post-process analysis, after all data has been gathered, to determine the best state estimates of the past given all gathered knowledge [34].

The smoothed estimate can be computed from the *posterior* estimate by propagating the Rauch-Tung-Striebel (RTS) differential equations

$$\bar{\boldsymbol{x}}_s' = \boldsymbol{f}(\bar{\boldsymbol{x}}_s, s) + Q_s \tilde{P}_s^{-1} (\bar{\boldsymbol{x}}_s - \tilde{\boldsymbol{x}}_s) \tag{16}$$

$$\bar{P}_s' = \left(F_s + Q_s \tilde{P}_s^{-1}\right) \bar{P}_s + \bar{P}_s \left(F_s + Q_s \tilde{P}_s^{-1}\right)^{\mathsf{T}} - Q_s \tag{17}$$

backward from arc-length ℓ to 0, with initial conditions $\bar{\boldsymbol{x}}_\ell = \tilde{\boldsymbol{x}}_\ell$ and $\bar{P}_\ell = \tilde{P}_\ell$.

3.2 Experimental Results

We applied the methods presented herein to a three-tube concentric-tube robot, modeled by Eqs. (3)–(6), and shown in Fig. 2i. The sensing system incorporates

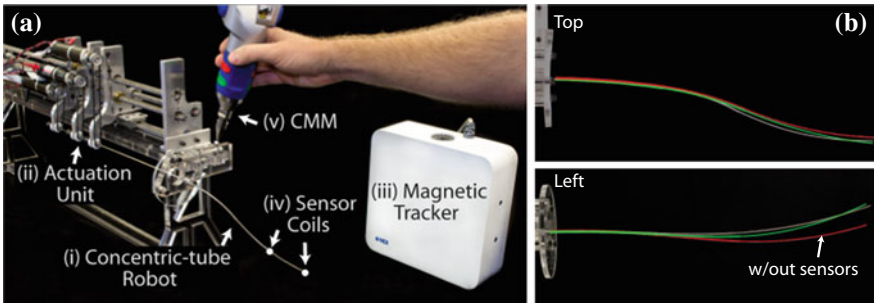

Fig. 2 **a** The experimental setup consists of a three-tube concentric-tube robot (*i*), controlled with a 6-DoF motorized actuation unit (*ii*), and with a electromagnetic sensing-system (*iii*) that tracks two sensor coils (*iv*) embedded in the robot's inner tube. A coordinate measuring machine (CMM) is used to obtain ground-truth measurements of the robot-tip position (*v*). **b** An example configuration of the concentric-tube robot with the shape (position) estimate, that incorporates magnetic position sensors, is shown with the shape estimate without magnetic position-sensors along with the actual shape of the robot. For the configuration shown, the tip-position errors were 7.3 and 16.0 mm for the estimate with and without sensor information, respectively

information from the six encoders of the actuation unit (Fig. 2ii) and an NDI Aurora electromagnetic-tracking system (Fig. 2iii) that measures the position of two sensing-coils placed in the concentric-tube robot as shown in Fig. 2iv. A FARO Gage coordinate measuring machine (Fig. 2v) was used to measure registration transformation between the robot and electromagnetic tracker as well as for obtaining ground-truth tip-position used in the experiments. We found that the six encoder measurements and the measured registration are sufficient to guarantee observability as discussed in Sect. 3.1, under the zero-tip-moment assumption ($\boldsymbol{\psi}_\ell'' = \mathbf{0}$).

The magnetic-tracker measurements add additional information that improves the state estimate under modeling uncertainty. We experimentally demonstrate their benefit by placing the concentric-tube robot in four configurations and comparing the error in tip-position provided by the smoothed estimate with the magnetic-tracker information to the smoothed estimate without tracker information. The tip-position error was measured using the CMM. On average, the accuracy of the smoothed estimate with and without tracker information was 8.8 and 14.5 mm, respectively. Figure 2b shows the shape estimate with and without the magnetic-tracking sensors for one of the four configurations used in our experiments.

The smoothed estimate for the states of the three-tube concentric-tube robot is implemented with the initial covariance of the tube-twist angles $\boldsymbol{\psi}_0$ set to $0.08I$ rad^2, where I is a 3×3 identity matrix, the initial proximal covariance of the tube-twist-angle rates-of-change $\boldsymbol{\psi}_0'$ are set to $0.01I$ (rad/m)^2, the initial proximal covariance of the backbone position $\boldsymbol{p}_0$ are set to $5 \times 10^{-5} I$ m^2. The covariances of the initial proximal backbone orientation (represented as a quaternion) and the concentric-tube translations $\boldsymbol{\sigma}_0$ are assumed to be zero. These initial covariances are found using estimates of calibration accuracy and are used as the initial values for the state-covariance in the computation of the posterior state-estimate obtained by integrating the Kalman-Bucy filter equations, (10) and(11). The position covariance of the magnetic tracker is experimentally found to be $1 \times 10^{-6} I$ m^2, which is used in the Kalman update step (12)–(15) for the posterior state-estimate.

4 Connections Between Estimation and Design, Sensing, and Planning

4.1 Connections Between Mechanical Design and Estimation

When the application requires the continuum robot to be sensed, the mechanical design of the robot plays an important role in estimation through the kinematic model (1)–(2), which is used in the Kalman-Bucy filter to condition the uncertain sensor observations. The mechanical design affects the quality of the state estimate (i.e., the covariance), through the linearized-kinematics state matrix F_s, which appears in differential equations (11) and (17) that govern the propagation of the prior and smoothed covariances along the length of the continuum robot. The physicall

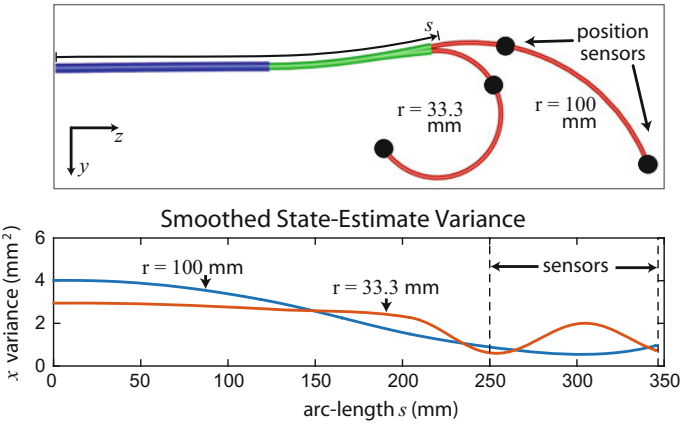

Fig. 3 The effect of changing a concentric-tube robot's inner-tube curvature on the smoothed state-estimate position variance in the x direction (out of the page) is shown (the variance in the y and z are largely unchanged). The smoothed estimate is found using the methods in Sect. 3.1 with two backbone-position sensors arranged on the robot as depicted. The covariances used by the smoothed estimator are for the physical robot reported in Sect. 3.2

properties of the robot that affect the matrix F_s could be, in the case of a tendon-actuated robot with a backbone, the robot's backbone stiffness or the distance of routed tendons to the backbone. In the case of a concentric-tube robot, physical properties can also include tube precurvatures and tube stiffnesses. The physica properties could vary along the length of the robot. For example, one or more flexure-hinges along the backbone (e.g., [50]) would locally decrease its stiffness.

As an example of how a continuum robot's mechanical design could affect state estimation, we study how changing the curvature of a concentric-tube robot's innermost tube changes the variance of the smoothed position estimate. We use two position sensors placed as shown in Fig. 3, with the methods of Sect. 3.1, using the robot and covariance parameters reported in Sect. 3.2. We now explore the effect on the covariance of changing the inner-tube's radius of curvature from 100 to 33.3 mm. The x-variance (out of the page) of the smoothed position estimate for each radius is shown in Fig. 3 (the variance in the y and z directions is largely unchanged), plotted as a function of backbone arc-length s. As indicated, the x variance increases between the two sensors (i.e., between arc-lengths at 250 and 350 mm) as the curvature increases. In this region, the robot's backbone position is most sensitive to rotation of the inner tube, which causes uncertainty in the inner-tube's rotation to manifest itself more in the backbone uncertainty, particularly in the x direction.

A nonintuitive effect occurs for proximal arc-lengths between 0 mm and approximately 150 mm. In this region, higher inner-tube curvature tends to reduce the x backbone-position variance. This could be an effect resulting from the geometry of the concentric-tube robot's proximal end and the sensor placements on the robot's backbone. Naturally, it would be difficult to maneuver a robot through a narrow

passageway in this configuration. In order to make the most of this effect, the robot's curvature should be designed in coordination with a motion planner in order to account for constraints imposed by the robot's environment.

4.2 Connections Between Sensor Selection, Sensor Placement, and Estimation

The question of what sensors should be chosen and their placement, is a frequent concern of continuum robot designers. Often there are space limitations due to the requirement that the diameter be small (e.g., to navigate through blood vessels) and there is little room left over once actuators have been installed. Therefore, it is desirable to obtain as much state information as possible, with as few sensors as possible.

The kinematic structure of the continuum robot, the robot's configuration, and the states that the sensors observe all contribute to the amount of state information obtained by the sensors. An example is shown for a concentric-tube robot in Fig. 4, where the smoothed state covariance in the x direction is shown for two arrangements of sensors. The covariance in the other two directions are largely unchanged. The covariances used by the smoothed estimator to obtain the results of Fig. 4 are for the physical robot reported in Sect. 3.2. Clearly, sensor placement has a large influence on the covariance of the smoothed backbone-position estimate. If an application requires the position estimate to be more accurate in the arc-length region (150, 300) mm, then placement "1" would be preferred over placement "2".

The variation in the smoothed covariance with variation in sensor placement can be exploited by the designer to best meet the needs of the application. The first task

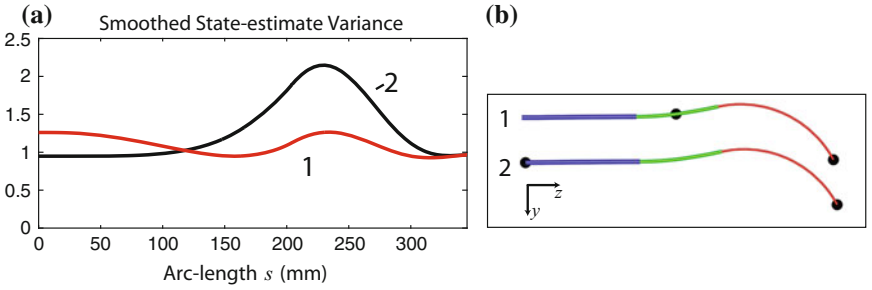

Fig. 4 The effect of changing sensor-observation placement is illustrated in this example where the smoothed state-estimate covariance in the x direction is shown (**a**) for two sensor arrangements (**b**). In *1* the one sensor is placed in the middle of the robot and one at the distal end, while in *2* one sensor is placed at the most proximal and most distal ends of the robot. The position-estimate covariance in the other two directions is largely unchanged. The covariances used by the smoothed estimator are for the physical robot reported in Sect. 3.2

is to select the appropriate sensors and sensor locations to achieve application specifications when states are estimated as described in Sect. 3.1. For many applications, partial state information may be sufficient. In others, accuracy requirements may vary by direction or arc-length. Based on such specifications, the methods in this paper enable one to determine how many sensors are required (e.g., to ensure observability described in Sect. 3.1).

One way to encode the requirements of the application is through a covariance-based metric, over which optimization in the sensor positions can be performed. If there are several arc-length points-of-interest $\gamma_1, \ldots, \gamma_j$ where the uncertainty of a continuum robot's state estimate is critical in specific directions (e.g., to ensure that the position estimate in the direction of nearest obstacles is highly certain), then an example of a metric on the smoothed covariance at the points-of-interest could be

$$\mathscr{U}(\bar{P}_{\gamma_1}, \ldots, \bar{P}_{\gamma_k}) = \max_{i=1\ldots j} \operatorname{tr}(E_i^{\mathsf{T}} \bar{P}_{\gamma_i} E_i) \tag{18}$$

where tr denotes the matrix trace, and E_i is a positive-semidefinite matrix used to select the critical directions of covariance, to selectively assign priority to arc-length the points-of-interest on the robot, or enforce unit-consistency. This metric minimizes the worst-case average estimate-variance at the arc-length points-of-interest.

4.3 Connections Between Motion Planning and Estimation

A major benefit of continuum robots is that they have the potential to snake through constrained spaces. The basic motion planning problem is to find a time-ordered sequence of continuum-robot inputs $\boldsymbol{u}_1(\boldsymbol{x}_0), \ldots, \boldsymbol{u}_k(\boldsymbol{x}_0)$, for time indices $1 \cdots k$, that guide the robot through the constrained space without colliding with obstacles in the environment. Motion planning is particularly relevant to surgical applications of continuum robots, where physicians desire to reach a surgical target while avoiding anatomical obstacles (e.g., bones, blood vessels, and sensitive organs) or danger zones established by the physician that correspond to high risk areas.

To avoid obstacles, motion planners must have knowledge over time of the robot's state, which for continuum robots includes the robot's shape (e.g., position-curve parameterized by arc-length s). In practice, there is often substantial uncertainty in the estimate of the robot's shape, and the motion planner must account for the shape uncertainty to guarantee that obstacles will be avoided with a desired level of confidence. To address this challenge, rather than following the traditional workflow of computing a motion plan assuming perfect state estimation and then relying on a real-time controller to account for uncertainty, recent work has investigated integrating motion planning with control to compute motion policies, which are parameterized by time and sensor measurements. Combining motion planning, control, and state estimation into a single problem can result in higher quality plans. General motion planning methods linking these problems have been developed for robots for which

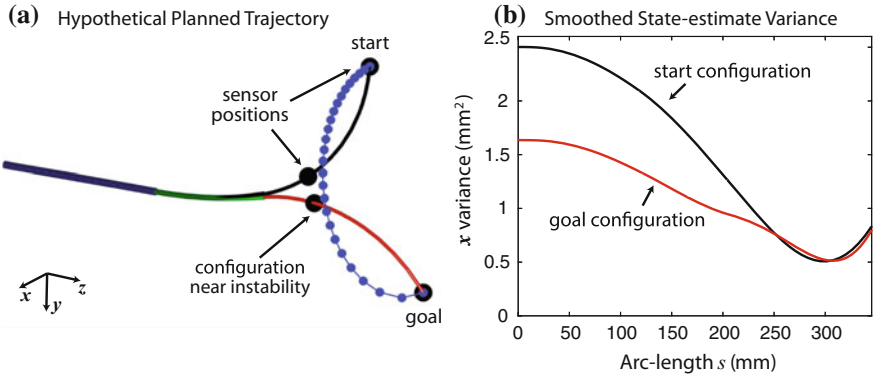

Fig. 5 The effect of changing the input $\boldsymbol{u}(\boldsymbol{x}_0)$ to follow a hypothetical trajectory from a start to goal configuration that could have been generated as an obstacle-avoiding trajectory by a motion planner. The variance in the x-direction of the concentric-tube robot's position-covariance is shown at both configurations. (The position-variance in the other directions are largely unchanged.) The covariances used by the smoothed estimator are for the physical robot reported in Sect. 3.2

state uncertainty can be modeled using Gaussian distributions in the state space. These belief-space planners, e.g., [6, 11, 20, 25–28, 45, 46], often use a sampling-based or optimization-based motion planner integrated with an automatically-tuned linear controller, and variants have been specifically applied to medical robots such as steerable needles and concentric-tube robots based on simplified uncertainty models [35, 36, 44]. Better models of the belief space of continuum robots (i.e., the space of distributions of state estimates given specific sensor measurements) could enable the computation of more effective motion policies.

For concentric-tube robots, some configurations naturally result in lower smoothed covariances than others. To illustrate the information available to a motion planner, Fig. 5 shows the smoothed state-estimate variance in the x direction as the physical concentric-tube robot from Sect. 3.2 follows a hypothetical trajectory, where the inner tube is rotated from the start-configuration to the end-configuration as shown in Fig. 5a. As the concentric-tube robots nears the goal-configuration, the smoothed variance of the robot's shape estimate in the x-direction decreases (the estimate improves) by 35% at the proximal end of the robot with little change in the distal end. The covariances used by the smoothed estimator are for the physical robot reported in Sect. 3.2. For motion planners to fully exploit the natural reduction in smoothed covariance, the temporal state transition and uncertainty in the transition must be understood and incorporated into a full spatiotemporal estimate. Creating efficient belief space planners for continuum robots that are based on accurate kinematic and uncertainty models is a significant research challenge.

Note that the covariance of the proximal position estimate represents the position uncertainty of the robot's pose in space. For some surgical applications, the robot's pose is could be intraoperatively registered to a patient's anatomy. The initial position covariance in the x direction for the experimental system in Sect. 3.2 (with which

Fig. 5 was computed) was estimated to be 50 mm^2. The process of Kalman smoothing can be used to improve the registration using the sensor observations taken along the robot's backbone. This is shown in Fig. 5, where position observations generated by the the electromagnetic tracker improve the position covariance of the registration in the x direction to less than 3.0 mm^2. In the case of the robot in the "goal" configuration, the covariance is improved to 1.6 mm^2. It may be beneficial for a motion planner to direct the robot near configurations where the initial registration can be improved before starting delicate surgical procedures.

When placed in certain configurations, some concentric-tube-robot designs exhibit elastic instability, which is observed as a windup, and sudden release of torsion. The release of torsion results in fast, uncontrolled motion of the robot's distal end. Passing through an elastic instability could be extremely harmful for sensitive surgical manipulation tasks. As a result, it is generally assumed that concentric-tube robots should be operated in configurations that are far from instability [3]. One nonintuitive result of Fig. 5, however, is that configurations near instabilities may be more "information rich" than those far away. This is indicated by the fact that the "goal" configuration, which is near what we understand to be the most likely configuration where instability occurs, has lower proximal position covariance than the "start" configuration, which is near what we know to be a configuration far from instability [14]. This indicates that configurations near instability may be useful for mitigating increases in the concentric-tube robot's state-estimate uncertainty as it follows a trajectory, and we expect that a motion planner that explicitly considers uncertainty could favor configurations near (but not at) instability at times for this reason.

5 Conclusion

In this paper, we used statistical state estimation as a tool to study the problems of designing a continuum robot's geometry, selecting and placing sensors for detecting the continuum robot, and using motion planning to direct the trajectory of a continuum robot to accomplish a task. These three problems are fundamentally coupled and their interaction can be studied using the covariance produced by statistical state estimation. The future of continuum robots lies in the simultaneous solution to the continuum-robot design, sensing, and planning problems in order to produce continuum-robot systems that make the most of their geometry and available information to satisfy the needs of the most demanding applications.

References

1. Ayvali, E., Liang, C.-P., Mingyen, H., Chen, Y., Desai, J.P.: Towards a discretely actuated steerable cannula for diagnostic and therapeutic procedures. Int. J. Rob. Res. **31**(5), 588–603 (2012)
2. Baykal, C., Torres, L.G., Alterovitz, R.: Optimizing design parameters for sets of concentric tube robots using sampling-based motion planning. In: Proceedings of IEEE/RSJ International Conference on Intelligent Robots and Systems, pp. 4381–4387 (2015)
3. Bergeles, C., Dupont, P.E.: Planning stable paths for concentric tube robots. In: Proceedings of IEEE/RSJ International Conference on Intelligent Robots and Systems, pp. 3077–3082 (2013)
4. Bergeles, C., Gosline, A.H., Vasilyev, N.V., Codd, P.J., del Nido, P.J., Dupont, P.E.: Concentric tube robot design and optimization based on task and anatomical constraints. IEEE Trans. Robot. **31**(1), 67–84 (2015)
5. Borum, A., Matthews, D., Bretl, T.: State estimation and tracking of deforming planar elastic rods. In: Proceedings of IEEE International Conference on Robotics and Automation, pp. 4127–4132 (2014)
6. Bry, A., Roy, N.: Rapidly-exploring random belief trees for motion planning under uncertainty. In: Proceedings of IEEE International Conference on Robotics and Automation, pp. 723–730 (2011)
7. Bryson, C.E., Rucker, D.C.: Toward parallel continuum manipulators. In: Proceedings of IEEE International Conference on Robotics and Automation, pp. 778–785 (2014)
8. Burgner, J., Gilbert, H.B., Webster III, R.J.: On the computational design of concentric tube robots: incorporating volume-based objectives. In: Proceedings - IEEE International Conference on Robotics and Automation, pp. 1193–1198 (2013)
9. Burgner-Kahrs, J., Rucker, D.C., Choset, H.: Continuum robots for medical applications: a survey. IEEE Trans. Robot., (2015, in press)
10. Crassidis, J.L., Junkins, J.L.: Optimal Estimation of Dynamic Systems, 2nd edn. CRC Press, Boca Raton (2011)
11. Du, Toit, Noel, E., Burdick, J.W.: Robot motion planning in dynamic, uncertain environments. IEEE Trans. Robot. **28**(1), 101–115 (2012)
12. Dupont, P.E., Lock, J., Itkowitz, B., Butler, E.: Design and control of concentric-tube robots. IEEE Trans. Robot. **26**(2), 209–225 (2010)
13. Gilbert, H.B., Rucker, D.C., Webster III, R.J.: Concentric tube robots: state of the art and future directions. Proc. Int. Symp. Robot. Res., (2013, in press)
14. Gilbert, H.B., Hendrick, R.J., Webster, III., R.J.: Elastic Stability of Concentric Tube Robots. IEEE Trans. Rob. (2015)
15. Hannan, M.W., Walker, I.D.: Real-time shape estimation for continuum robots using vision. Robotica **23**(5), 645–651 (2005)
16. Hirose, S.: Biologically Inspired Robots, Snake-Like Locomotors and Manipulators. Oxford University Press, Oxcord (1993)
17. Jeon, J., Yi, B.-J.: Shape prediction algorithm for flexible endoscope. In: Proceedings of IEEE International Conference on Robotics and Automation, pp. 2856–2861 (2014)
18. Jones, B.A., Walker, I.D.: Kinematics for multisection continuum robots. IEEE Trans. Robot. **22**(1), 43–55 (2006)
19. Koolwal, A.B., Barbagli, F., Carlson, C., Liang, D.: An ultrasound-based localization algorithm for catheter ablation guidance in the left atrium. Int. J. Rob. Res. **29**(6), 643–665 (2010)
20. Lee, A., Duan, Y., Patil, S., Schulman, J., McCarthy, Z., van den Berg, J., Goldberg, K., Abbeel, P.: Sigma hulls for gaussian belief space planning for imprecise articulated robots amid obstacles. In: Proceedings of IEEE/RSJ International Conference on Intelligent Robots and Systems, pp. 5660–5667 (2013)
21. Lobaton, E.J., Fu, J., Torres, L.G., Alterovitz, R.: Continuous shape estimation of continuum robots using X-ray images. In: Proceedings of IEEE International Conference on Robotics and Automation, pp. 725–732 (2013)

22. Lyons, L.A., Webster III, R.J., Alterovitz, R.: Motion planning for active cannulas. In: Proceedings of IEEE/RSJ International Conference on Intelligent Robots and System, pp. 801–806 (2009)
23. Novotny, P.M., Stoll, J.A., Dupont, P.E., Howe, R.D.: Real-time visual servoing of a robot using three-dimensional ultrasound. In: Proceedings of IEEE International Conference on Robotics and Automation, pp. 2655–2660 (2007)
24. Odhner, L.U., Jentoft, L.P., Claffee, M.R., Corson, N., Tenzer, Y., Ma, R.R., Buehler, M., Kohout, R., Howe, R.D., Dollar, A.M.: A compliant, underactuated hand for robust manipulation. Int. J. Rob. Res. **33**(5), 736–752 (2014)
25. Patil, S., van den Berg, J., Alterovitz, R.: Motion planning under uncertainty in highly deformable environments. In: Proceedings of Robotics: Science and Systems (2011)
26. Patil, S., van den Berg, J., Alterovitz, R.: Estimating probability of collision for safe motion planning under gaussian motion and sensing uncertainty. In: Proceedings of IEEE International Conference on Robotics and Automation, pp. 3238–3244 (2012)
27. Platt Jr., R., Tedrake, R., Kaelbling, L., Lozano-Perez, T.: Belief space planning assuming maximum likelihood observations. In: Proceedings of Robotics: Science and Systems (2010)
28. Prentice, S., Roy, N.: The belief roadmap: efficient planning in belief space by factoring the covariance. Int. J. Rob. Res. **28**(11), 1448–1465 (2009)
29. Roesthuis, R.J., Kemp, M., van den Dobbelsteen, J.J., Misra, S.: Three-dimensional needle shape reconstruction using an array of fiber bragg grating sensors. IEEE/ASME Trans. Mech. **19**(4), 1115–1126 (2014)
30. Rucker, D.C., Webster, R.J.: Statics and dynamics of continuum robots with general tendon routing and external loading. IEEE Trans. Robot. **27**(6), 1033–1044 (2011)
31. Rucker, D.C., Jones, B.A., Webster III, R.J.: A geometrically exact model for externally loaded concentric-tube continuum robots. IEEE Trans. Robot. **26**(5), 769–780 (2010)
32. Ryu, S.C., Dupont, P.E.: FBG-based shape sensing tubes for continuum robots. In: Proceedings IEEE International Conference on Robotics and Automation, pp. 3531–3537 (2014)
33. Ryu, S.C., Quek, Z.F., Koh, J.-S., Renaud, P., Black, R.J., Moslehi, B., Daniel, B.L., Cho, K.-J., Cutkosky, M.R.: Design of an optically controlled mr-compatible active needle. IEEE Trans. Robot. **31**(1), 1–11 (2015)
34. Simon, D.: Optimal State Estimation: Kalman, H_∞, and Nonlinear Approaches. Wiley, New Jersey (2006)
35. Sun, W., Alterovitz, R.: Motion planning under uncertainty for medical needle steering using optimization in belief space. In: Proceedings of IEEE/RSJ International Conference on Intelligent Robots and Systems, pp. 1775–1781 (2014)
36. Sun, W., Torres, L.G., van den Berg, J., Alterovitz, R.: Safe motion planning for imprecise robotic manipulators by minimizing probability of collision. In: Proceedings of International Symposium Robotics Research (2013)
37. Swaney, P.J., Burgner, J., Pheiffer, T.S., Rucker, D.C., Gilbert, H.B., Ondrake, J.E., Simpson, A.L., Burdette, E.Clif, Miga, M.I., Webster III, R.J.: Tracked 3D ultrasound targeting with an active cannula. In: Proceedings of the Society of Photo-Optical Instrumentation Engineers, pp. 83160R–83160R–9 (2012)
38. Thrun, S., Burgard, W., Fox, D.: Prob. Robot. MIT Press, Cambridge (2006)
39. Torres, L.G., Alterovitz, R.: Motion planning for concentric tube robots using mechanics-based models. In: Proceedings of IEEE/RSJ International Conference on Intelligent Robots and Systems, pp. 5153–5159 (2011)
40. Torres, L.G., Webster III, R.J., Alterovitz, R.: Task-oriented design of concentric tube robots using mechanics-based models. In: Proceedings of IEEE/RSJ International Conference on Intelligent Robots and Systems, pp. 4449–4455 (2012)
41. Torres, L.G., Baykal, C., Alterovitz, R.: Interactive-rate motion planning for concentric tube robots. In: Proceedings of IEEE International Conference on Robotics and Automation, pp. 1915–1921 (2014)
42. Torres, L.G., Kuntz, A., Gilbert, H.B., Swaney, P.J., Hendrick, R.J., Webster III, R.J., Alterovitz, R.: A motion planning approach to automatic obstacle avoidance during concentric tube robot

teleoperation. In: Proceedings of the IEEE International Conference on Robotics and Automation, pp. 2361–2367 (2015)
43. Trovato, K., Popovic, A.: Collision-free 6D non-holonomic planning for nested cannulas. In: Proceedings of SPIE Medical Imaging, vol. 7261 (2009)
44. van den Berg, J., Patil, S., Alterovitz, R., Abbeel, P., Goldberg, K.: LQG-based planning, sensing, and control of steerable needles. In: Hsu, D. et al. (eds), Algorithmic Foundations of Robotics IX. Springer Tracts in Advanced Robotics, vol. 68, pp. 373–389. Springer, Heidelberg (2010)
45. van den Berg, J., Abbeel, P., Goldberg, K.: LQG-MP: optimized path planning for robots with motion uncertainty and imperfect state information. Int. J. Rob. Res. **30**(7), 895–913 (2011)
46. van den Berg, J., Patil, S., Alterovitz, R.: Motion planning under uncertainty using iterative local optimization in belief space. Int. J. Rob. Res. **31**(11), 1263–1278 (2012)
47. Webster III, R.J., Jones, B.A.: Design and kinematic modeling of constant curvature continuum robots: a review. Int. J. Rob. Res. **29**(13), 1661–1683 (2010)
48. Xu, K., Simaan, N.: Analytic formulation for kinematics, statics, and shape restoration of multibackbone continuum robots via elliptic integrals. ASME J. Mech. Robot. **2**(1), 011006 (2009)
49. Xu, R., Patel, R.V.: A fast torsionally compliant kinematic model of concentric-tube robots. In: Proceedings of International Conference IEEE Engineering in Medicine and Biology Society, pp. 904–907 (2012)
50. York, P., Swaney, P.J., Gilbert, H.B, Webster III, R.J.: A wrist for needle-sized surgical robots. In: Proceedings of IEEE International Conference on Robotics and Automation, pp. 1776–1781 (2015)